HETEROCYCLES, Vol. 104, No. 3, 2022, pp. 495 - 511. © 2022 The Japan Institute of Heterocyclic Chemistry
Received, 16th November, 2021, Accepted, 20th December, 2021, Published online, 22nd December, 2021
DOI: 10.3987/COM-21-14592

A NEW C,C-LINKED FUNCTIONALIZED BIPYRAZOLE: SYNTHESIS, CRYSTAL STRUCTURE, SPECTROSCOPIES AND DFT STUDIES. EVALUATION OF THE ANTIBACTERIAL ACTIVITY AND CATALYTIC PROPERTIES

Ibrahim Bouabdallah,[1] Tarik Harit,[1]* Yahya Rokni,[2] Mahmoud Rahal,[3] Monique Tillard,[4] Driss Eddike,[1] Abdeslam Asehraou,[2] and Fouad Malek[1]*

[1] Laboratory of Applied Chemistry and Environment, Faculty of Sciences, Mohammed First University Bd Mohamed VI, 60 000 Oujda, Morocco. t.harit@ump.ac.ma, fouad_malek@yahoo.fr; [2] Laboratory of Bioresources, Biotechnology, Ethnopharmacology and Health, Faculty of Sciences, Mohamed 1st University, Oujda 60000, Morocco; [3] Laboratory of Chemical Physics, Faculty of Sciences, Chouaib Doukkali University, BP 20, 24000, El Jadida, Morocco; [4] ICGM, Univ. Montpellier, CNRS, ENSCM, Montpellier, France

Abstract – The synthesis of new C,C-linked functionalized bipyrazole is reported. Its molecular structure has been confirmed by spectroscopic and spectrometric methods and its single crystal structure determined by X-ray analysis. The ligand **2** has been subjected to DFT and TD-DFT theoretical calculations and results are consistent with the experimental chemical analyses. The compound possesses no antibacterial activity up to 256 μg/mL. However, its complexes with copper(II) salts are found to be good catalysts for the oxidation of 3,5-di-*tert*-butylcatechol (DTBC) into 3,5-di-*tert*-butylquinone (DTBQ) with a rate varying from 9.58 $\mu mol \cdot L^{-1} \cdot min^{-1}$ for the **2**-$[Cu(MeCO_2)_2]$ complex to 5.27 $\mu mol \cdot L^{-1} \cdot min^{-1}$ for the **2**-$[Cu(BF_4)_2]$ complex.

INTRODUCTION

The bipyrazolic derivatives constitute an important group of intermediates in the synthesis of a number of compounds. These heterocyclic compounds exhibit a wide range of application areas. They are known as potential antimicrobial,[1] antitumor[2] or anti-inflammatory[3] agents, they can play a role in corrosion processes,[4] behave as enzyme selective inhibitors,[5] be effective catalysts in specific chemical reactions[6-9]

or substances acting as chemo-sensors for copper(II) in aqueous solution.[10] The bipyrazole compounds are also capable to form stable complexes with transition metals as copper(II), cobalt(II) and ruthenium(II).[11] Furthermore, they have been evaluated as immobilized proton carrier inside proton exchange membranes for PEMFC fuel cells.[12]

Among the bipyrazolic derivatives that have earlier attracted some attention, are the particular C,C-linked bipyrazole derivatives.[13] Within this family, compounds differ by the nature of substituents on the pyrazole rings which considerably affects their energetic[14,15] and biological[16] properties.

As a part of our research program, we concentrated our efforts on the synthesis of C,C-linked functionalized bipyrazole compounds in which the alkylation is going to take place at the β position of the R group (Figure 1), in order to study the impact on catalytic and biological activities as well on extraction of transition metal cations.

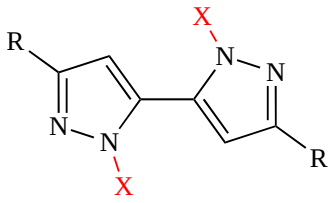

Figure 1. Structure of β N-alkylated C,C-linked bipyrazole derivatives

Thus, we describe in the present paper, the synthesis and the characterization of a new bipyrazolic compound, namely 1,1'-di(2-hydroxyethyl)-3,3'-diisopropyl-5,5'-bipyrazole **2**. Its solid state structure has been determined from single crystal X-ray diffraction and its antimicrobial activity, catalytic properties have been examined. Density Functional Theory (DFT) calculations have been also carried out to take better insight into the spectroscopic, geometrical and electronic properties of compound **2**.

RESULTS AND DISCUSSION

2-1. Synthesis of 1,1'-di(2-hydroxyethyl)-3,3'-diisopropyl-5,5'-bipyrazole **2**

To obtain the target compound **2**, we condensed two equivalents of 2-hydroxyethylhydrazine and one equivalent of 3,8-dihydroxy-2,9-dimethyldeca-3,7-diene-5,6-dione **1**[17] in ethanol at room temperature. This reaction led to a major product which is not, as evidenced by thin layer chromatography (TLC), the 1,1'-di(2-hydroxyethyl)-5,5'-diisopropyl-3,3'-bipyrazole **2'**.[18] Indeed the isomer **2'** was obtained as minor product. Generally, this kind of reaction can give a mixture of three position isomers represented in Scheme 1, in proportions depending on the experimental conditions.

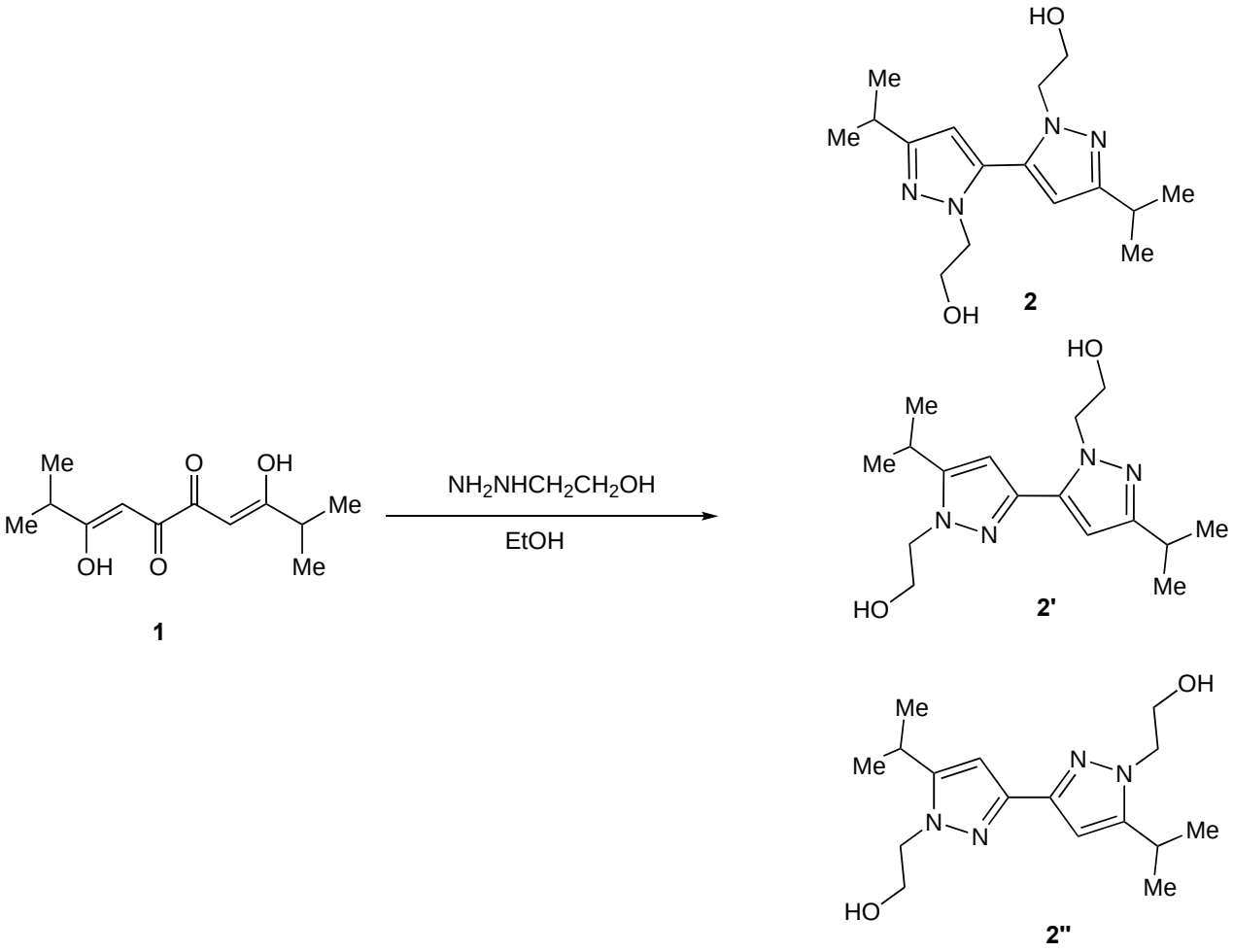

Scheme 1. Possible isomers resulting from the condensation of **1** and 2-hydroxyethylhydrazine

These isomers should be easily differentiated using ^{13}C NMR spectroscopy.[19,20] However, in the current case, the ^{13}C NMR spectrum of the product is found very close to that of 1,1'-di(2-hydroxyethyl)-5,5'-diisopropyl-3,3'-bipyrazole.[18] The ^{1}H NMR spectroscopy also gives similar results as well as mass spectrometry making these tools unable to evidence the structure of the obtained isomer. To overcome these issues, the resulting compound was recrystallized in an equi-volume mixture of diethyl ether and dichloromethane in order to produce single crystals for a subsequent X-ray crystallographic analysis that evidenced the ligand **2** in the product.

2-2. Description of the crystal structure

The asymmetric unit of formula $C_8H_{13}N_2O$ consists in a substituted pyrazole ring bearing a $-CH_2-CH_2-OH$ chain at nitrogen N1 atom and an isopropyl group at C5 atom. Equivalent atoms are generated using the symmetry operation *i* (*x*, *-y*, *½-z*) to complete the molecule which is represented in Figure 1 and corresponds to the formula $C_{16}H_{26}N_4O_2$. The atom positional and equivalent displacement parameters are listed in Table 1.

Table 1. Atomic coordinates ($\times 10^4$) and equivalent isotropic displacement parameters ($Å^2 \times 10^3$). U_{eq} is defined as one third of the trace of the orthogonalized U_{ij} tensor.

	x	y	z	U_{eq}
N1	1105(1)	533(2)	2667(1)	35(1)
N2	1603(1)	903(2)	3239(1)	37(1)
O1	1639(1)	-4838(2)	1635(1)	50(1)
C1	1319(1)	-3477(3)	2189(1)	51(1)
C2	1425(1)	-834(3)	2083(1)	39(1)
C3	322(1)	1312(2)	2775(1)	33(1)
C4	316(1)	2238(3)	3444(1)	38(1)
C5	1126(1)	1958(3)	3710(1)	36(1)
C6	1492(1)	2780(3)	4399(1)	45(1)
C7	965(1)	2047(4)	5004(1)	76(1)
C8	1639(2)	5461(4)	4393(1)	80(1)

The molecule of **2** is formed with two substituted pyrazole rings, interlinked *via* C3 - C3^i bonds. Note that, according to the symmetry of C2/c space group, the molecule is non-centrosymmetric. Moreover, its conformation is such that the hydroxyethyl chains are placed on the same side of the molecular mean-plane as illustrated by the molecular representation in the *ab* plane (*b* vertical axis) given as an inset in Figure 2.

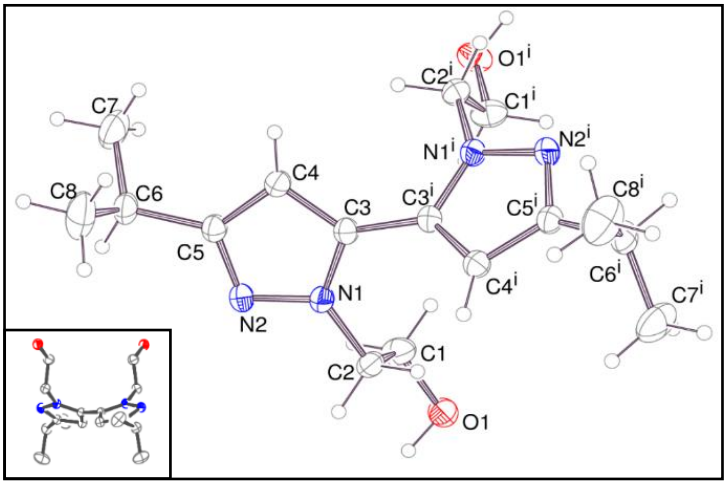

Figure 2. Representation of the $C_{16}H_{26}N_4O_2$ molecule with ellipsoids at 30% probability. The symmetry code used to generate equivalent atoms is *i:* x, -y, ½-z. The view in *ab* plane (inset) makes clearer the molecule conformation.

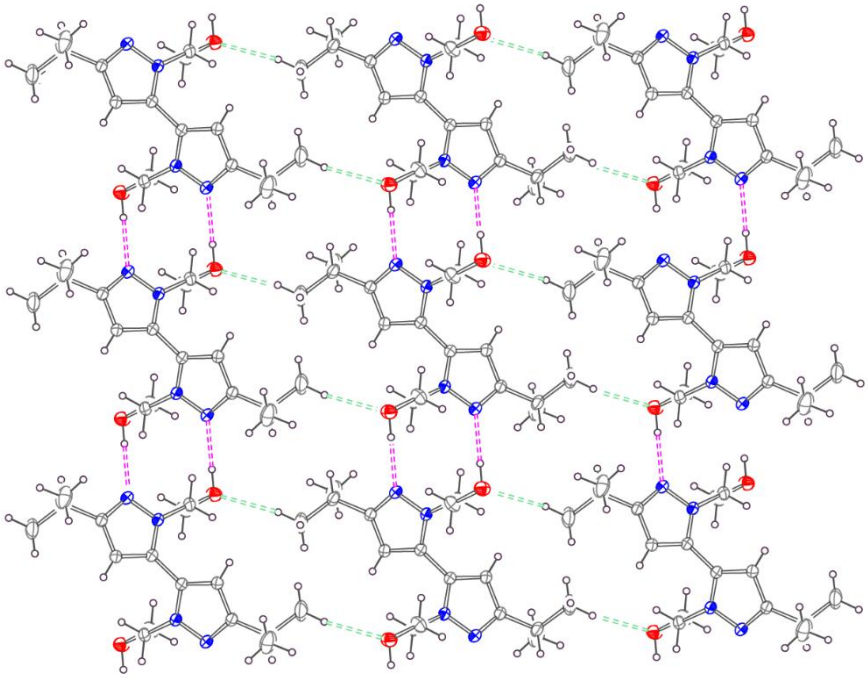

Figure 3. Projection of the molecular packing in the monoclinic cell (along *b* unique axis) highlighting the weak intermolecular interactions

The monoclinic lattice contains four molecules $C_{16}H_{26}N_4O_2$ stacked in the crystal with their mean plane nearly perpendicular to the unique *b*-axis (Figure 3). The separation between two molecules in this direction is 5.57Å. The molecular arrangement is characterized with intermolecular interactions with neighboring units through hydrogen-type contacts O1–H1···N2 of 2.867Å, angle 176° (dotted pink lines). For the larger distances, with 3.546Å at O1···H4–C4 (angle 140°) and 3.631Å at O1···H7b–C7 (angle 168°), the intermolecular interactions rather belong to the van der Waals forces category (dotted green lines). Nevertheless, all these weak intermolecular interactions are likely to stabilize the compound in its crystallized state. The intermolecular binding energy which is responsible for this stabilization, especially involving hydrogen bonds, has been evaluated at ~58 kcal.mole^{-1} from additional DFT calculations (Dmol^3, given in supplementary material) performed both for the molecule and the crystal.

2-3. FTIR and UV-Visible spectroscopy

The experimental FTIR spectrum of compound **2** is presented in Figure 4 while the corresponding calculated spectrum is given in Figure S1 (see supporting information).

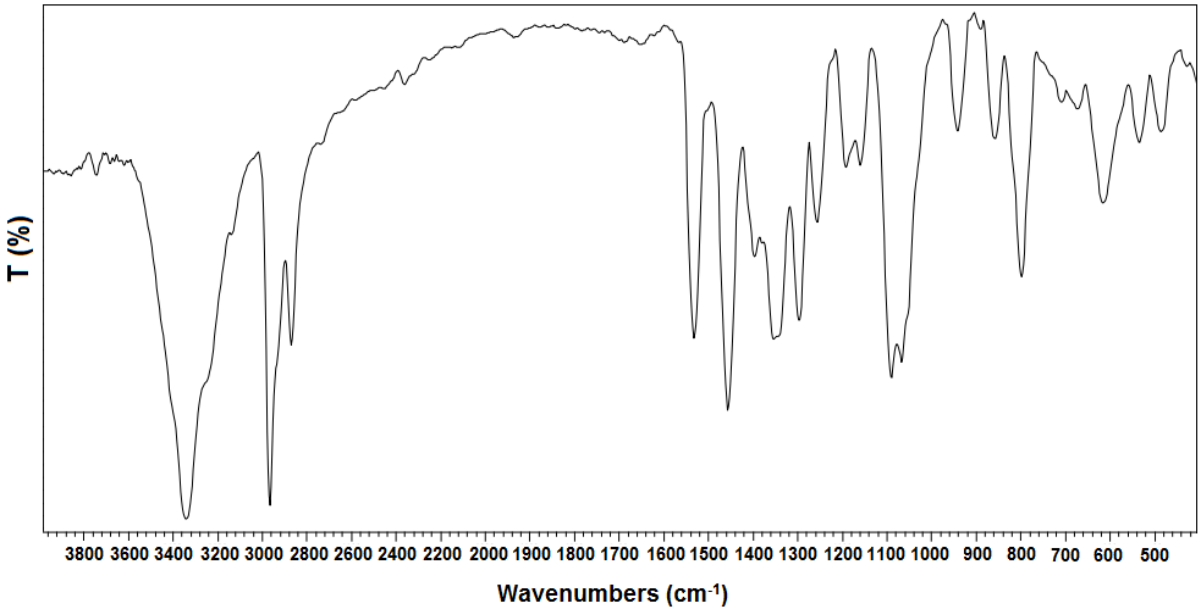

Figure 4. FTIR spectrum of compound **2**

The experimental spectrum shows an intense pic at 3347 cm^{-1} attributed to the O-H stretching vibration. The same vibration is observed at 3562 cm^{-1} on the theoretical spectrum calculated by the DFT/B3LYP method. This difference may be due the strong intermolecular hydrogen bonding as already observed for other compounds.[21] The C-H aliphatic and aromatic stretching vibrations appear in the range 2976-2691 cm^{-1} while, they were calculated between 3147 and 2670 cm^{-1}. The characteristic bands corresponding to $\nu_{C=C}$ and $\nu_{C=N}$ vibrations of the pyrazolic ring occur in the range 1352-1534 cm^{-1} while they are calculated in the range 1269-1569 cm^{-1}. Finally the C-O band, theoretically expected at 1049 cm^{-1} is observed at 1058 cm^{-1}.

In addition, the electronic absorption spectrum was also recorded for this compound in methanol (Figure 5). In good agreement with the calculated spectrum (Figure S2 in the supporting information), it displays two bands in the 350-200 nm region resulting from the π–π* and the n–π* transitions.[22]

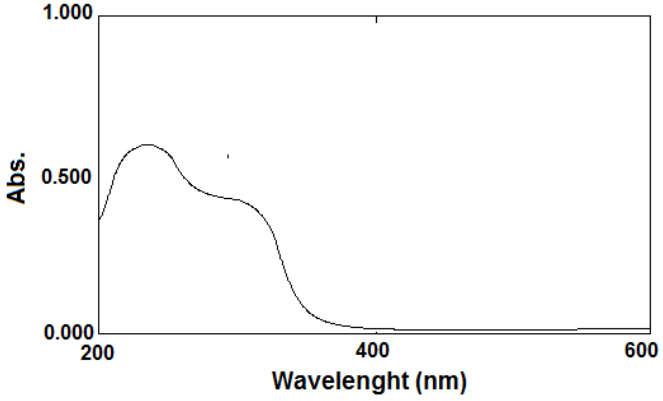

Figure 5. Experimental UV-Visible spectrum of bipyrazolic compound **2**

2-4. NMR spectroscopy

The ^{1}H and ^{13}C chemical shifts with respect to tetramethylsilane (TMS) in $CDCl_3$ solvent have been calculated using the DFT method and B3LYP/6 311++G(d,p) basis set. They are listed in Table 2 comparatively with the experimental values measured for the chemical shifts. It must be pointed out that the calculated and experimental values are very similar as proved by the correlation coefficients of 0.991 and 0.968 calculated for the ^{1}H NMR and ^{13}C NMR spectroscopies, respectively.

For the experimental ^{1}H NMR spectrum, the chemical shift values are observed in the range 1.06-6.34 ppm, while they are theoretically predicted from 1.27 to 5.93 ppm. Two triplets at 4.14 and 4.03 ppm in the ^{1}H NMR experimental spectrum correspond to the ethylene group hydrogens and are associated to the calculated values of 3.95 and 3.89 ppm. A singlet observed at 6.39 ppm has been assigned to pyrazolic proton, the corresponding calculated position being at 6.16 ppm.

Table 2. Comparison of the experimental and calculated ^{1}H and ^{13}C NMR chemical shift values (in ppm) for compound **2**

^{1}H NMR (in $CDCl_3$)			^{13}C NMR (in $CDCl_3$)		
Atoms	δ_{exp}	$\delta_{calc.}$ B3LYP 6-311++G(d,p)	Atoms	$\delta_{exp.}$	$\delta_{calc.}$ B3LYP 6-311++G(d,p)
$CH(Me)_2$	1.26	1.27	$CH(\underline{Me})_2$	22.90	23.42
$C\underline{H}(Me)_2$	2.97	2.98	$\underline{C}H(Me)_2$	25.64	33.25
$NCH_2C\underline{H}_2OH$	4.03	3.84	$N\underline{C}H_2CH_2OH$	50.21	51.62
$NC\underline{H}_2CH_2OH$	4.14	3.60	$CH_2\underline{C}H_2$-OH	62.31	63.75
C4-$\underline{H}$	6.39	5.93	C4	99.67	103.09
			C5	145.78	134.48
			C3	151.33	159.66
R^2	0.991		R^2	0.968	

On the other hand, chemical shifts in the ^{13}C NMR experimental and calculated spectra appear in the range 151.33-22.99 ppm and 159.66-23.44 ppm, respectively. Two signals observed at 50.21 and 62.31 ppm in the experimental spectrum have been attributed to the two carbon atoms of the hydroxyethyl chain. The corresponding signals are calculated at 51.62 and 63.75 ppm. One more signal observed at 99.67 ppm in the experimental spectrum has been associated with the signal calculated at 103.09 ppm and assigned to the atom C4 of the pyrazole ring.

2-5. DFT calculations

As shown above, the combination of the B3LYP functional with the 6-311++G(d,p) basis set which is used in the calculations provides the best agreement between the calculated and experimental values both for the ^{1}H and ^{13}C-NMR chemical shifts. Moreover, these results are consistent with the structure determined from X-ray diffraction crystal data. The full geometry optimizations performed in DFT calculations are based on the minimization of the total energy (TE) and provide some useful parameters as the electric dipole moment (μ_M) and the one-electron energies of the frontier molecular orbitals.

The electric dipole moment is a measure of the overall polarity and it describes the distribution of electrons in a molecule.[23] It is also used as a good predictor of the molecule stability in solution.[24] The value of the electric dipole moment is 1.55 D for the current molecule and it is higher than that reported for 3,3'-diisopropyl-5,5'-bipyrazole.[25] Therefore, compound **2** will be all the most favored in solvents with high dielectric constant.

The HOMO (highest occupied molecular orbital) and LUMO (lowest unoccupied molecular orbital) one-electron energies have been used to calculate the global theoretical reactivity parameters for compound **2** according to formulas given in the literature.[25]

Table 3 summarizes all the calculated quantities: electric dipole moment (μ_M), various energy levels (TE, HOMO, LUMO, gap) and following indices: ionization energy (I), electron affinity (A), electronegativity (χ), chemical hardness (η), softness (σ), electronic chemical potential (μ) and global electrophilicity index (ω).

Table 3. Total energy, frontier orbital energies and reactivity indices for compound **2**

Method	B3LYP/ 6-311++G(d,p)
Total Energy (Hartree)	-995.0732778
E_{HOMO} (Hartree)	-0.25
E_{LUMO} (Hartree)	-0.04
Gap (eV)	5.74
μ_M (debye)	1.58
I (eV)	6.79
A (eV)	1.05
χ (eV)	3.92
η (eV)	2.87
σ	0.35
μ (eV)	-3.92
ω (eV)	2.67

The electronegativity measures the resistance of a molecule to an electron loss. Instead, the stabilization of a molecule by acquisition of an additional charge from its environment can be evaluated by the global electrophilicity index[25] which has also been tested as a possible descriptor for toxicology prediction.[26] With a high value of 2.67 eV for the electrophilicity index ω, the molecule is characterized with a strong electrophile character.

Chemical hardness (η) and softness (σ) are interesting quantities associated to the molecular stability and reactivity.[27] Basically, the chemical hardness denotes the resistance of a molecule (ion or atom) against the deformation or the polarization of the electronic cloud under small perturbation occurring during chemical reaction. Thus, hard and soft molecules are respectively linked to large and small gap energies.[25] The energy gap is then used as an indicator for the chemical reaction and its value of 5.74 eV indicates a high stability for the current molecule **2**. The gap which is the difference in energy between the frontier orbitals is found very close for the 1,1'-di(2-hydroxyethyl)-3,3'-diisopropyl-5,5'-bipyrazole (**2**) and the 3,3'-diisopropyl-5,5'-bipyrazole, leading to remark the weak influence of the 1-hydroxyethyl substituent. As hardness and softness are directly correlated with the energy gap, their values η of 2.88 eV and σ of 0.35 eV are not modified either when a 1-hydroxyethyl chemical group is substituted on the pyrazole ring in the 3,3'-diisopropyl-5,5'-bipyrazole molecule.

Plots of the frontier molecular orbital (FMO) and molecular electrostatic potential surface (MEPS) are shown in Figure 6. For the HOMO and LUMO orbitals, positive and negative regions are represented in red and green, respectively. The MEPS isolevel representation has been generated for the optimized geometry using the GaussView 5.0.8 software. Red zones correspond to the most positive, green zones to zero and blues zones to the most negative electrostatic potentials.

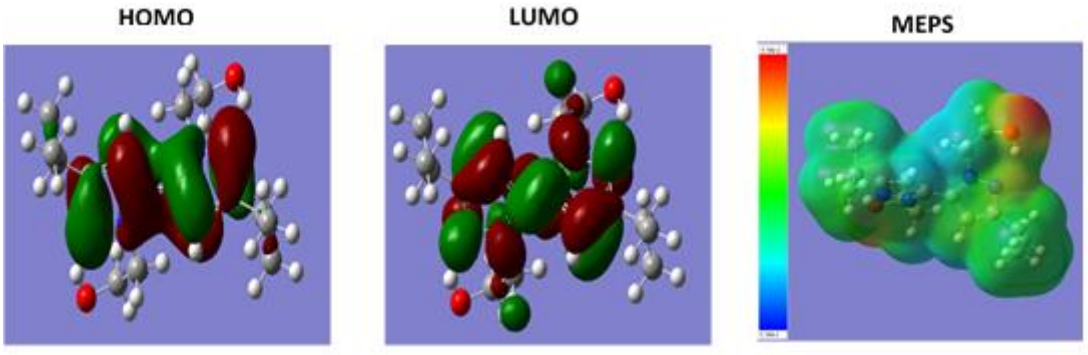

Figure 6. The FMO and MEPS for molecule **2** calculated at B3LYP/ 6-311++g(d,p) level

The HOMO energy is related to the affinity to donate electrons to appropriate acceptors while the LUMO energy indicates the ability for the molecule to accept electrons. The frontier orbitals determine the way that the molecule interacts with other species, and their energies are associated with the electron-donating

(HOMO) and the electron-accepting (LUMO) abilities of the molecule.[28] The HOMO is located close to the nitrogen atoms which can act as electron donors. Instead, the LUMO is distributed over the main ring molecular skeleton.

The molecular electrostatic potential surface (MEPS) allows to visualize the charge distributions and is an useful tool to evaluate the regio-selectivity of molecules.[29,30] With high potential values, the regions around the oxygen atoms are characterized as the most electron-rich in molecule **2**, thus they are the favored centers for an electrophilic attack. On the contrary, the most negative potentials are mainly localized over pyrazolic hydrogen atoms which are possible sites for a nucleophilic attack.

2-6. Antibacterial activity

The in vitro antibacterial potency of the bipyrazolic compound **2** was examined against two Gram negative bacteria (*Escherichia coli* and *Pseudomonas aeruginosa*) and three Gram-positive bacteria (*Listeria innocua*, *Micrococcus luteus* and *Staphylococcus aureus*) by measuring minimum inhibitory concentrations (MICs). In this study, Gentamicin was used as a positive control. As shown in Table 4, Gentamicin displays MIC values of 1 μg/mL for *Micrococcus luteus*, *Pseudomonas aeruginosa* and *Escherichia coli* and 2 μg/mL for *Staphylococcus aureus* and *Listeria innocua*.

Table 4. In vitro antibacterial activity (MIC, μg/mL) of the bipyrazolic compound **2**

	Gram-positive bacteria			Gram-negative bacteria	
	Micrococcus luteus	*Staphylococcus aureus*	*Listeria innocua*	*Pseudomonas aeruginosa*	*Escherichia coli*
Compound **2**	>256	>256	>256	>256	>256
Gentamicin	1	2	2	1	1

Although it bears in its structure isopropyl and alcohol groups, two fragments which could improve the antibacterial potency,[30,31] the compound **2** displays no antibacterial activity up to 256 μg/mL for all the tested bacteria. This unexpected result may be explained by the weak electrophilic character of the hydroxyl hydrogen atom and the position of the strong electrophilic sites as evidenced by the MEPS. For these reasons, it is reasonable to think that compound **2** cannot easily interact with the bacterial cytoplasmic membrane.

2-7. Catecholase activity

In order to assess the catalytic properties of Cu complex with compound **2**, the catalytic potency of *in situ* generated copper complexes was tested in the oxidation reaction of catechol derivatives. First, progress of the oxidation reaction of 3,5-di-*tert*-butylcatechol was checked in absence of **2** and practically no variation

in absorbance was recorded. Then, measurements were conducted at identical experimental conditions, in presence of **2** to evaluate the ability of the different copper complexes to catalyze the reaction. The catalytic activity concentrations are given in Table 5.

Table 5. Kinetic data for the oxidation of 3,5-di-*tert*-butylcatechol by ligand 2-copper(II) complexes

Salts	Catalytic activity concentrations ($\mu mol \cdot L^{-1} \cdot min^{-1}$)
$CuCl_2$	5.27
$Cu(MeCO_2)_2$	9.58
$Cu(NO_3)_2$	9.10
$Cu(BF_4)_2$	5.27

The results demonstrate that all the *in situ* complexes of ligand **2** catalyze the oxidation reaction of 3,5-di-*tert*-butylcatechol into 3,5-di-*tert*-butylquinone with reaction rates varying from 9.58 $\mu mol \cdot L^{-1} \cdot min^{-1}$ in case of **2**-[$Cu(MeCO_2)_2$] complex to 5.27 $\mu mol \cdot L^{-1} \cdot min^{-1}$ for **2**-[$Cu(BF_4)_2$]. The reactivity for this oxidation reaction decreases in the order $MeCO_2^- > NO_3^- > BF_4^- = Cl^-$. Two types of anions can be distinguished, Cl^- and BF_4^- anions combine with the molecule to give complexes in which the accessibility to the metal center is made difficult for the substrate. This leads to a lowering of the catalytic activity. The second group comprises the anions $MeCO_2^-$ and NO_3^- which give complexes with higher catalytic activity probably resulting from of a high substrate-to-complex adequacy.

In summary, we have prepared and characterized a new C,C-linked functionalized bipyrazole 1,1'-di(2-hydroxyethyl)-3,3'-diisopropyl-5,5'-bipyrazole (**2)** by condensation of 1-hydroxyethylhydrazine with 3,8-dihydroxy-2,9-dimethyldeca-3,7-diene-5,6-dione in ethanol. The resulting compound display no antibacterial activity up to 256 μg/mL. Nevertheless, the *in situ* complexes of ligand **2** with copper(II) are able to catalyze the oxidation reaction of 3,5-di-*tert*-butylcatechol (DTBC) to 3,5-di-*tert*-butylquinone (DTBQ) by atmospheric oxygen.

EXPERIMENTAL

3-1. Reagents and instruments

The reagents 1-hydroxyethylhydrazine (95%), EtOH, CH_2Cl_2 and Et_2O were purchased from Sigma-Aldrich and used without further purification. Melting point was determined in open glass capillaries using BÜCHI 510 Melting Point apparatus and is given as measured without any correction. The infrared (IR) spectra was recorded on a PERKIN-ELMER 1310 infrared spectrophotometer using the KBr disk technique.

The NMR spectra (^{1}H, ^{13}C) were recorded on a BRUKER 300 NMR spectrometer operating at 300 MHz for ^{1}H and at 75 MHz for ^{13}C. Chemical shifts are listed in ppm and reported relatively to tetramethylsilane (TMS) taken as internal standard. Splitting patterns are labelled as follows with s: singlet, d: doublet, t: triplet and m: multiplet. Mass spectra were obtained on a VG7070E spectrometer. UV-Vis spectra were recorded on Shimadzu Europe - UV-1650PC.

3-2. Synthesis of the ligand **2**

To a solution of tetraketone **1** (13.8 mmol) in EtOH (20 mL), was added 1-hydroxyethylhydrazine (27.6 mmol). The mixture was agitated at room temperature for 2 h. The solvent was then removed under reduced pressure. The residue was purified and crystals were obtained by recrystallization from an equi-volume mixture of Et_2O and CH_2Cl_2.

Yield: 70%; mp 220-221 °C; R_f = 0.25 [silica: CH_2Cl_2/EtOH (9:1)]; ^{1}H NMR (Figure S3) (300 MHz, $CDCl_3$, δ, ppm): 6.39 (s, 2H, C4-H), 4.14 (t, 4H, NCH_2CH_2OH, *J* = 5.1Hz), 4.03 (t, 4H, NCH_2CH_2OH, *J* = 5.1 Hz), 2.94 (m, 2H, $CH(CH_3)_2$), 1.26 (d, 12H, $CH(CH_3)_2$, *J* = 6.9Hz); ^{13}C NMR (Figure S4) (75 MHz, $CDCl_3$, δ, ppm): 151.33 (C3), 145.78 (C5), 99.67 (C4), 62.13 (N-CH_2CH_2OH), 50.21 (CH_2CH_2-OH), 25.64 ($CH(CH_3)_2$), 22.90 ($CH(CH_3)_2$); IR (KBr, cm^{-1}): 3347 (ν_{O-H}), 2976 (ν_{C-H}), 1534 ($\nu_{C=N}$), 1352 ($\nu_{C=C}$), 1058 (δ_{C-O}). MS (Figure S5) (ESI): *m/z* = 307.2 $[M+1]^+$.

3-3. X-Ray diffraction and structure solution

The compound was obtained as colorless platelets displaying beveled edges. A nice-looking specimen was selected using a stereomicroscope equipped with a polarizing filter. After checking of its single-crystal nature, it was used for X-ray diffraction intensity measurements (Mo-Kα radiation, λ = 0.71073 Å) at room temperature on an Xcalibur (Oxford Diffraction, Abingdon, Oxfordshire, England) four circle CCD diffractometer. The data reduction was performed using CrysAlis software[32] and the unit cell determined by least-squares from the entire reflection data set. Lorentz and polarization corrections were applied to intensities of the 9705 collected reflections. Structure has been solved and refined with the SHELX-2013 program package.[33] Full-matrix least-squares refinements on F^2 were carried out using a set of 1551 unique reflections of which 1194 are observed according to the criterion $I > 2\sigma(I)$. Positional and anisotropic displacement parameters were refined for all non-H atoms. The hydroxyl H-atom, detected in the final Fourier difference, has been freely refined with an isotropic displacement parameter. The other hydrogen atoms have been generated and refined using AFIX instructions with isotropic displacement parameters equal to 1.2 times (1.5 for terminal CH_3) the U_{eq} of the parent atom. Table 6 reports the main crystal data and refinement parameters. The structure representations are drawn with ORTEP-3 for windows.[34]

Table 6. Crystal data and structure refinement for $C_{16}H_{26}N_4O_2$

Formula, M, Z	$C_{16}H_{26}N_4O_2$, 306.40, 4
Temperature	293 (2) K
Space group	Monoclinic, C 2/c (n° 15)
Lattice	a = 16.105(6), b = 5.5774(6), c = 19.114(2) Å
	β = 91.21(2), α = γ = 90°
Crystal	0.29 × 0.17 × 0.07 mm
θ range	3.27 to 25.23°
Reflections	1551 unique [R_{int} = 2.17%], 1194 observed
Final R indices [I>2 σ(I)]	R1 = 0.0377, wR2 = 0.1005
R indices (all data)	R1 = 0.0503, wR2 = 0.1051
Δρ Fourier residuals	0.168 / -0.187 e.Å^{-3}

3-4. Quantum chemical calculation

Density functional theory (DFT) at B3LYP/6-311++G(d,p) computational level[35-39] has been used to calculate the quantum chemical parameters for the studied compound **2**. The Gaussian 03W package has been chosen to perform the geometry optimizations[40,41] without any symmetry constraints. The harmonic frequencies were calculated to ensure that the structures really correspond to a true local minimum energy on the potential energy surface. GaussView 5.0.8 visualization program[42] was employed to develop the molecular structure, total electron density, molecular electrostatic potential surface (MEPS) maps and UV-visible spectra. The chemical shifts theoretically expected have been calculated with the gauge including atomic orbital (GIAO) method.[43,44] Solvent effects were calculated within the PCM (Polarizable Continuum Model) approximation.[45-47] Transformation of absolute shielding values into chemical shifts has been carried out according to the following equations[48]:

$$\delta^1H = 31.0 - 0.97 \times \sigma^1H$$

$$\delta^{13}C = 175.7 - 0.963 \times \sigma^{13}C$$

3-5. Antibacterial activity evaluation

The minimum inhibitory concentration (MIC) measurement has been realized to examine the antibacterial activity of compound **2** against three Gram positive bacteria (*Staphylococcus aureus, Micrococcus luteus* and *Listeria innocua*) and two Gram negative bacteria (*Escherichia coli* and *Pseudomonas aeruginosa*) following the same protocol as given in our previous works.[49] Mother solutions of compound **2** and Gentamicin (positive control) in DMSO (1 mg/mL) were diluted at concentrations of 32, 64, 128 and 254

μg/mL. The overnight cultures of the target bacteria, 10 μL of the Mueller Hinton Broth (MHB) of about 2 10^6 CFU/mL of tested bacteria, were inoculated in 2 mL of MHB containing different concentrations of the tested compound with gentamicin at neutral pH and then were incubated at 37 °C for 12 h. The MICs values were considered as the lowest concentrations of the compound for which no visible bacterial turbidity was noticed.

3-6. Catecholase activity measurements

Kinetic measurements were made by spectrophotometry using an UV-Visible Cecil CE 292 Digital Spectrophotometer, by following the appearance of 3,5-di-*tert*-butylquinone over time at 25 °C (400 nm maximal absorbance, $\varepsilon = 1600\ M^{-1}\cdot cm^{-1}$ in methanol). The metal complex prepared in *situ* from a copper salt and the ligand (0.3 mL of 10^{-3} M MeOH solution) and 2 mL of a solution (10^{-1} M MeOH solution) of 3,5-di-*tert*-butylcatechol were added together in the spectrophotometric cell. The catalytic activity concentration (b) has been calculated from the slope of the tangent to the curve of absorbance versus time, according to the following equation[50]:

$$b = (\Delta A / \Delta t) \times (V_{react} / V_{comp}) \times (\varepsilon \,.\, L)^{-1} \times 10^6$$

where b, $\Delta A/\Delta t$, V_{react}, V_{comp}, ε and L are respectively the catalytic activity concentration, the slope of the tangent to the curve, the total reaction volume (V_{react} = 2.3 mL), the volume of solution containing the metal (V_{comp} = 0.3 mL), the molar absorption coefficient and the path length of the beam-light through the solution (1 cm).

REFERENCES AND NOTES

1. F. Abrigach and R. Touzani, *Med. Chem. (Los Angeles)*, 2016, **6**, 292.
2. F. Malek, N. Draoui, O. Feron, and S. Radi, *Res. Chem. Intermed.*, 2014, **40**, 681.
3. S. Domiati, M. Mehanna, H. Ragab, H. N. Chmaisse, and A. El Mallah, *J. Inflamm. Res.*, 2018, **11**, 143.
4. H. Elmsellem, T. Harit, A. Aouniti, F. Malek, A. Riahi, A. Chetouani, and B. Hammouti, *Prot. Met. Phys. Chem. Surf.*, 2015, **51**, 873.
5. T. Harit, F. Malek, B. El Bali, A. Khan, K. Dalvandi, B. P. Marasini, S. Noreen, R. Malik, S. Khan, and M. I. Choudhary, *Med. Chem. Res.*, 2012, **21**, 2772.
6. S. Shin, S. Nayab, and H. Lee, *Polyhedron*, 2018, **141**, 309.
7. S. Choi, S. H. Ahn, S. Nayab, and H. Lee, *Inorg. Chim. Acta*, 2015, **435**, 313.
8. T. Harit, H. Abouloifa, M. Tillard, D. Eddike, A. Asehraou, and F. Malek, *J. Mol. Struct.*, 2018, **1163**, 300.
9. S. O. Ojwach and J. Darkwa, *Inorg. Chim. Acta*, 2010, **363**, 1947.
10. J. Isaad, T. Harit, H. Bessbousse, A. El Achari, and F. Malek, *Chem. Afr.*, 2019, **2**, 29.

11. I. Alkorta, R. M. Claramunt, E. Diez-Barra, J. Elguero, A. de la Hoz, and C. Lopez, *Coord. Chem. Rev.*, 2017, **339**, 153.
12. T. Harit, B. Ameduri, and F. Malek, *Solid State Ion.*, 2018, **317**, 108.
13. I. Bouabdallah, T. Harit, M. Rahal, F. Malek, M. Tillard, and D. Eddike, *Acta Chim. Slov.*, 2021, **68**, 718.
14. D. Kumar, Y. Tang, C. He, G. H. Imler, D. A. Parrish, and J. N. M. Shreeve, *Chem. Eur. J.*, 2018, **24**, 17220.
15. I. L. Dalinger, K. Y., Suponitsky, T. K. Shkineva, D. B. Lempert, and A. B. Sheremetev, *J. Mater. Chem. A*, 2018, **6**, 14780.
16. Y. L. Li, J. Zhuo, and S. Mei, Bipyrazole derivatives as jak inhibitors, U.S. Patent No. 9,926,301. Washington, DC: U.S. Patent and Trademark Office, 2018.
17. I. Bouabdallah, I. Zidane, F. Malek, R. Touzani, M. El Kodadi, and A. Ramdani, *Molbank*, 2003, **2003**, M345.
18. I. Bouabdallah, I. Zidane, B. Hacht, A. Ramdani, and R. Touzani, *J. Mater. Environ. Sci.*, 2010, **1**, 20.
19. M. Begtrup, G. Boyer, P. Cabildo, C. Cativiela, R. M. Claramunt, J. Elguero, J. I. García, C. Toiron, and P. Veds, *Magn. Reson. Chem.*, 1993, **31**, 107.
20. M. Cherfi, I. Dib, T. Harit, A. Ziyyat, and F. Malek, *Drug Dev. Res.*, 2021, **82**, 1055.
21. S. Sebastian and N. Sundaraganesan, *Spectrochim. Acta A*, 2010, **75**, 941.
22. T. Harit, M. Dahmani, S. Gaamouche, F. Malek, M. Dusek, A. Manseri, A. Asehraou, and B. El bali, *J. Mol. Struct.*, 2019, **1176**, 110.
23. F. E. T. Heakal, S. K. Attia, S. A. Rizk, M. A. AbouEssa, and A. E. Elkholy, *J. Mol. Struct.*, 2017, **1147**, 714.
24. M. A. Monge, E. G. Puebla, J. Elguero, C. Toiron, and W. Meutermans, *Spectrochim. Acta A*, 1994, **50**, 727.
25. I. Bouabdallah, M. Rahal, T. Harit, A. El Hajbi, F. Malek, D. Eddike, M. Tillard, and A. Ramdani, *Chem. Phys. Lett.*, 2013, **588**, 208.
26. D. R. Roy, R. Parthasarathi, B. Maiti, V. Subramanian, and P. K. Chattaraj, *Bioorg. Med. Chem.*, 2005, **13**, 3405.
27. J. Melin, F. Aparicio, M. Galván, P. Fuentealba, and R. Contreras, *J. Phys. Chem. A*, 2003, **107**, 3831
28. E. H. Avdović, D. Milenković, J. M. D. Marković, J. Đorović, N. Vuković, M. D. Vukić, V. V. Jevtić, S. R. Trifunović, I. Potočňák, and Z. Marković, *Spectrochim. Acta A*, 2015, **195**, 31.
29. P. Politzer and J. S. Murray, *Theor. Chem. Acc.*, 2002, **108**, 134.

30. T. Harit, R. Bellaouchi, A. Asehraou, M. Rahal, I. Bouabdallah, and F. Malek, *J. Mol. Struct.*, 2017, **1133**, 74.
31. H. Yamamura, A. Miyagawa, H. Sugiyama, K. Murata, T. Mabuti, R. Mitsuhashi, T. Hagiwara, M. Nonaka, K. Tanimoto, and H. Tomita, *ChemistrySelect*, 2016, **1**, 469.
32. Rigaku Oxford Diffraction, CrysAlisPro Software system, version 1.171.38.41, Rigaku Corporation, Oxford, UK., 2015.
33. G. M. Sheldrick, 'SHELXS. A program for crystal structures solution; shelxl. a program for refining crystal structures', University of Göttingen, Germany, 2013.
34. L. J. Farrugia, *J. Appl. Crystallogr.*, 2012, **45**, 849.
35. A. D. Becke, *Phys. Rev. A*, 1988, **38**, 3098.
36. A. D. Becke, *J. Chem. Phys.*, 1993, **98**, 5648.
37. C. Lee, W. Yang, and R. G. Paar, *Phys. Rev. B*, 1988, **37**, 785.
38. R. G. Parr and W. Wang, 'Density-functional theory of atoms and molecules', Oxford University Press, New York, 1994.
39. R. Neumann, R. H. Nobes, and N. C. Handy, *Mol. Phys.*, 1996, **87**, 1.
40. M. J. Frisch, G. W. Trucks, H. B. Schlegel, G. E. Scuseria, M. A. Robb, J. R. Cheeseman, J. A. Montgomery, Jr., T. Vreven, K. N. Kudin, J. C. Burant, J. M. Millam, S. S. Iyengar, J. Tomasi, V. Barone, B. Mennucci, M. Cossi, G. Scalmani, N. Rega, G. A. Petersson, H. Nakatsuji, M. Hada, M. Ehara, K. Toyota, R. Fukuda, J. Hasegawa, M. Ishida, T. Nakajima, Y. Honda, O. Kitao, H. Nakai, M. Klene, X. Li, J. E. Knox, H. P. Hratchian, J. B. Cross, V. Bakken, C. Adamo, J. Jaramillo, R. Gomperts, R. E. Stratmann, O. Yazyev, A. J. Austin, R. Cammi, C. Pomelli, J. W. Ochterski, P. Y. Ayala, K. Morokuma, G. A. Voth, P. Salvador, J. J. Dannenberg, V. G. Zakrzewski, S. Dapprich, A. D. Daniels, M. C. Strain, O. Farkas, D. K. Malick, A. D. Rabuck, K. Raghavachari, J. B. Foresman, J. V. Ortiz, Q. Cui, A. G. Baboul, S. Clifford, J. Cioslowski, B. B. Stefanov, G. Liu, A. Liashenko, P. Piskorz, I. Komaromi, R. L. Martin, D. J. Fox, T. Keith, M. A. Al-Laham, C. Y. Peng, A. Nanayakkara, M. Challacombe, P. M. W. Gill, B. Johnson, W. Chen, M. W. Wong, C. Gonzalez, and J. A. Pople, 'Gaussian03, Revision C.02', Wallingford CT: Gaussian Inc., 2003.
41. N. Tokay, Z. Seferoğlu, C. Öğretir, and N. Ertan, *ARKIVOC*, 2008, **xv**, 9.
42. R. D. Dennington, T. A. Keith, and J. M. Millam, 'GaussView 5', Gaussian Inc., 2008.
43. R. Ditchfield, *Mol. Phys.*, 1974, **27**, 789.
44. F. London, *J. Phys. Radium*, 1937, **8**, 397.
45. S. Miertus, E. Scrocco, and J. Tomasi. *Chem. Phys.*, 1981, **55**, 117.
46. J. Tomasi and M. Persico, *Chem. Rev.*, 1994, **94**, 2027.

47. B. Mennucci and R. Cammi, 'Continuum solvation models in chemical physics: from theory to applications', John Wiley & Sons, Chichester, 2007.
48. I. Alkorta, J. Elguero, M. Pérez-Torralba, C. López, and R. M. Claramunt, *Magn. Reson. Chem.*, 2015, **53**, 353.
49. T. Harit, M. Cherfi, H. Abouloifa, J. Isaad, I. Bouabdallah, M. Rahal, and F. Malek, *Polycycl. Aromat. Compd.*, 2020, **40**, 1459.
50. B. Baudin, Méthodes de mesure des activités enzymatiques, Biophysique, chimie organique et chimie analytique.
https://www.remede.org/librairie-medicale/pdf/e9791090018273. (Accessed 15 November 2021)